Magnetic helicity transport in the advective gauge family

Simon Candelaresi,[1,2] Alexander Hubbard,[1] Axel Brandenburg,[1,2] and Dhrubaditya Mitra[1]
[1]*NORDITA, AlbaNova University Center, Roslagstullsbacken 23, SE-10691 Stockholm, Sweden*
[2]*Department of Astronomy, Stockholm University, SE 10691 Stockholm, Sweden*

(Received 29 October 2010; accepted 14 December 2010; published online 10 January 2011)

Magnetic helicity fluxes are investigated in a family of gauges in which the contribution from ideal magnetohydrodynamics takes the form of a purely advective flux. Numerical simulations of magnetohydrodynamic turbulence in this advective gauge family exhibit instabilities triggered by the build-up of unphysical irrotational contributions to the magnetic vector potential. As a remedy, the vector potential is evolved in a numerically well behaved gauge, from which the advective vector potential is obtained by a gauge transformation. In the kinematic regime, the magnetic helicity density evolves similarly to a passive scalar when resistivity is small and turbulent mixing is mild, i.e., when the fluid Reynolds number is not too large. In the dynamical regime, resistive contributions to the magnetic helicity flux in the advective gauge are found to be significant owing to the development of small length scales in the irrotational part of the magnetic vector potential.
 [doi:10.1063/1.3533656]

I. INTRODUCTION

Most astrophysical and laboratory plasmas are good conductors. This, together with high-speed flows and large length scales, nearly universal in the astrophysical context, makes for large magnetic Reynolds numbers. In the limit of infinitely large magnetic Reynolds number, and for domains with closed boundaries, total magnetic helicity is a conserved quantity. Here, an analogy can be drawn with mass conservation in domains whose boundaries are closed to mass flux. Furthermore, in open domains, the change in total mass is governed by the mass flux across open surfaces. In ideal magnetohydrodynamics (MHD), a similar property holds for the total magnetic helicity. But unlike mass, magnetic helicity depends on the choice of gauge. In the special case of the advective gauge, the magnetic helicity flux is given by the velocity times the magnetic helicity density,[1] making this gauge particularly interesting for studying pointwise properties of magnetic helicity. This is an important goal of this paper.

Magnetic helicity plays an important role in many fields of plasma physics and astrophysics, and has applications ranging from tokamaks and other plasma confinement machines, to dynamo action in the Sun and the galaxy. Our physical understanding of the role of magnetic helicity in MHD is greatly aided by concepts such as Taylor relaxation,[2] selective decay,[3] and the inverse cascade of magnetic helicity.[4]

Furthermore, magnetic helicity is a crucial ingredient of the turbulent dynamos which are believed to be the source of the equipartition magnetic fields in astrophysical bodies such as stars and galaxies.[5] In all such cases the characteristic length scales of the dynamo generated magnetic field exceed those of the fluid's energy carrying scale. In dynamo theory, the formation of such a large-scale magnetic field is typically possible through the α effect, which is nonzero for helical turbulent flows. In periodic boxes with helical turbulence, the α effect becomes strongly quenched when the (appropriately normalized) magnetic helicity in the small-scale field (i.e., scales that are smaller than the energy-carrying scale of turbulent fluid) is comparable to the helicity in the small-scale velocity. Conservation of magnetic helicity implies that the helicity in small- and large-scale fields will have comparable magnitudes, so the quenching of the large-scale dynamo will occur for weak large-scale fields. This α quenching[6,7] increases with scale separation and endures for as long as magnetic helicity is nearly conserved, a resistive time that scales with the magnetic Reynolds number $\mathrm{Re}_M \equiv UL/\eta$. The quenching is called "catastrophic" because for the Sun $\mathrm{Re}_M \sim 10^9$ and the galaxy $\mathrm{Re}_M \sim 10^{15}$, and their resistive timescales are problematically long. This rapid preresistive saturation of the dynamo generated field poses clear difficulties in applying theory to astronomical systems, but it may be possible to alleviate the problem through magnetic helicity fluxes.[8,9] It should also be pointed out that problems with catastrophic quenching are often not clearly seen in present-day simulations.[10–12] While trend lines suggest that catastrophic quenching will occur, simulations at currently achievable, low to intermediate Re_M and scale separation have shown significant large-scale fields.

There exists reasonable observational evidence is support of such fluxes of magnetic helicity. The Sun's surface magnetic field shows helical structures.[13,14] Further, it was shown[15] that the S-shaped (helical) regions which are active in the corona are precursors of coronal mass ejections (CMEs) and later[16] that those regions are more likely to erupt. This suggests that the Sun sheds magnetic helicity via CMEs. Since the Sun's large-scale magnetic field is believed to be generated by a helical dynamo[17,18] this shedding of magnetic helicity could play an important role in the 11 year solar cycle. Physically, magnetic helicity fluxes out of the domain can be mediated in many ways, such as the aforementioned CMEs for the Sun[19] or fountain flows in the case of galaxies.[17] In direct simulations magnetic helicity fluxes

are permitted by adjusting the boundary conditions, e.g., to vertical field boundaries, but their actual presence can be difficult to ascertain. Internal helicity fluxes have also been found to alleviate α quenching[18] in systems with internal boundaries that separate zones of oppositely signed kinetic and magnetic helicities.

A difficulty in addressing the generation and transport of magnetic helicity is its gauge dependence. We denote the magnetic vector potential as $\boldsymbol{A}$ such that $\boldsymbol{B}\equiv\boldsymbol{\nabla}\times\boldsymbol{A}$ is the magnetic field. Magnetic helicity $H\equiv\int_V \boldsymbol{A}\cdot\boldsymbol{B}dV$ is independent of the gauge for perfectly conducting boundaries, as well as periodic boundaries so long as $\boldsymbol{A}$ is also required to be periodic. However, if one wishes to study the transport of magnetic helicity for physically motivated systems a nonvolume integral formulation will be needed. Magnetic helicity *density*, $h\equiv\boldsymbol{A}\cdot\boldsymbol{B}$, the quantity we will be working with, clearly depends on the gauge choice for $\boldsymbol{A}$. The gauge dependence of fluxes of mean magnetic helicity contained in the fluctuating fields was examined via direct numerical simulations (DNS) for three different gauges,[20] and it was found that, averaged over time, they do not depend on the gauge choice. This is a result of the fact that, for sufficient scale separation, the magnetic helicity of the fluctuating field can be expressed as the density of linkages, which in turn is gauge-invariant.[21] This result implies that the study of specific but useful gauge choices is a meaningful task.

In this work we examine the properties of magnetic helicity density in a particularly interesting gauge-family which we call "advective" because in this gauge the effect of velocity on the evolution equation of magnetic helicity takes the form of a purely advective term. In previous work[1] this gauge choice was shown to be crucial to understanding magnetic helicity fluxes in the presence of shear, including the Vishniac–Cho flux.[22] Unfortunately, evolving $\boldsymbol{A}$ in this gauge proves numerically unstable. This may be related to earlier findings in smoothed particle MHD calculations.[23,24] There, the problem was identified as the result of an unconstrained evolution of vector potential components, which were argued to be connected with "poor accuracy with respect to "reverse-advection"-type terms."[23] Our present work clarifies that this instability is related to the excessive build-up of irrotational contributions to the magnetic vector potential. These contributions have no physical meaning, but discretization errors at small length scales can spoil the solution dramatically.

We shall therefore describe a novel method for obtaining $\boldsymbol{A}$ in this gauge by evolving it first in a numerically robust gauge and then applying a gauge transformation with a simultaneously evolved gauge potential. This will be referred to as the Λ method throughout the text. Next, we show that the magnetic helicity density in the advective gauge tends to be small even pointwise, provided turbulent effects are still weak, and discuss the analogy with passive scalar transport. We conclude by pointing out that resistive terms break the analogy with passive scalar advection through the emergence of a turbulently diffusive magnetic helicity flux.

II. MAGNETIC EVOLUTION EQUATIONS

A. Weyl and advective gauges

In this work we remain within nonrelativistic MHD and hence neglect the Faraday displacement current. So the current density is given by $\boldsymbol{J}=\boldsymbol{\nabla}\times\boldsymbol{B}$, where $\boldsymbol{B}$ is the magnetic field and we use units where the vacuum permeability is unity. At the core of MHD is the induction equation

$$\frac{\partial\boldsymbol{B}}{\partial t}=\boldsymbol{\nabla}\times(\boldsymbol{U}\times\boldsymbol{B}-\eta\boldsymbol{J}), \tag{1}$$

where $\boldsymbol{U}$ is the velocity and η is the molecular magnetic diffusivity. Equation (1) can be uncurled to give an evolution equation for the magnetic vector potential $\boldsymbol{A}$, but only up to a gauge choice. In the Weyl gauge, indicated by a superscript W on the magnetic vector potential, we just have

$$\frac{\partial\boldsymbol{A}^W}{\partial t}=\boldsymbol{U}\times\boldsymbol{B}-\eta\boldsymbol{J} \tag{2}$$

but by adding the gradient of a scalar field, the vector potential can be obtained in any other gauge. Of particular interest to this paper is the advective gauge

$$\boldsymbol{A}^a=\boldsymbol{A}^W+\boldsymbol{\nabla}\Lambda^{W:a}, \tag{3}$$

where $\Lambda^{W:a}$ is the gauge potential that transforms from $\boldsymbol{A}^W$ to $\boldsymbol{A}^a$. We demand that[25]

$$\frac{DA_i^a}{Dt}=-U_{j,i}A_j^a-\eta J_i. \tag{4}$$

Here, $D/Dt=\partial/\partial t+\boldsymbol{U}\cdot\boldsymbol{\nabla}$ is the advective derivative. Consequently one can show that $\Lambda^{W:a}$ obeys the evolution equation (see Appendix A)

$$\frac{D\Lambda^{W:a}}{Dt}=-\boldsymbol{U}\cdot\boldsymbol{A}^W. \tag{5}$$

Thus, to obtain $\boldsymbol{A}^a$, one can either solve Eq. (4) directly or, alternatively, solve Eq. (2) together with Eq. (5) and use Eq. (3) to obtain $\boldsymbol{A}^a$. A possible initial condition for $\Lambda^{W:a}$ would be $\Lambda^{W:a}=0$, in which case $\boldsymbol{A}^a=\boldsymbol{A}^W$ initially. For numerical reasons that will be discussed in more detail below, we shall consider the indirect method of obtaining the magnetic vector potential in the advective gauge, but starting from more numerically stable gauge which will be discussed in Sec. II B.

Variants on the advective gauge have seen significant use, particularly in DNS with constant imposed shear. Although the magnetic field in such simulations must obey shearing-periodic boundary condition the vector potential need not. In particular, the evolution Eq. (2) does not impose shearing-periodicity on the vector potential, while Eq. (4) does, enabling shearing-periodic numerical simulations[26] in terms of $\boldsymbol{A}$.

For our purposes, the importance of Eq. (4) lies in the form of the magnetic helicity density evolution equation. By writing the induction equation in the form

$$\frac{DB_i}{Dt} = + U_{i,j}B_j - (\boldsymbol{\nabla}\cdot\boldsymbol{U})B_i - (\boldsymbol{\nabla}\times\eta\boldsymbol{J})_i \tag{6}$$

computing $D(\boldsymbol{A}^a\cdot\boldsymbol{B})/Dt=\boldsymbol{A}^a\cdot D\boldsymbol{B}/Dt+\boldsymbol{B}\cdot D\boldsymbol{A}^a/Dt$, and noting that the $A_iU_{i,j}B_j$ terms from both equations cancel, we find that

$$\frac{Dh^a}{Dt} = -h^a\,\boldsymbol{\nabla}\cdot\boldsymbol{U} - \boldsymbol{\nabla}\cdot(\eta\boldsymbol{J}\times\boldsymbol{A}^a) - 2\eta\boldsymbol{J}\cdot\boldsymbol{B} \tag{7}$$

which shows that in ideal MHD ($\eta=0$) under the assumption of incompressibility ($\boldsymbol{\nabla}\cdot\boldsymbol{U}=0$) the magnetic helicity density in the advective gauge, $h^a=\boldsymbol{A}^a\cdot\boldsymbol{B}$ is just advected with the flow like a passive scalar, i.e.,

$$\frac{Dh^a}{Dt} = 0 \quad (\text{for } \eta=0 \text{ and } \boldsymbol{\nabla}\cdot\boldsymbol{U}=0). \tag{8}$$

In the general case with $\boldsymbol{\nabla}\cdot\boldsymbol{U}\neq 0$, the rate of change of the local value of h^a is given by $-\boldsymbol{\nabla}\cdot(h^a\boldsymbol{U})$, which is analogous to the continuity equation for the fluid density. However, for $\eta\neq 0$, there is also a source term

$$\frac{\partial h^a}{\partial t} = -2\eta\boldsymbol{J}\cdot\boldsymbol{B} - \boldsymbol{\nabla}\cdot\boldsymbol{F}^a, \tag{9}$$

as well as a resistive contribution to the magnetic helicity flux

$$\boldsymbol{F}^a = h^a\boldsymbol{U} + \eta\boldsymbol{J}\times\boldsymbol{A}^a. \tag{10}$$

In this paper we address the question how the $\eta\boldsymbol{J}\times\boldsymbol{A}^a$ contribution scales in the limit $\eta\to 0$, i.e., for large values of Re_M. It could either stay finite, just like the resistive energy dissipation $\eta\boldsymbol{J}^2$, which tends to a finite limit[5] as $\eta\to 0$, or it could go to zero like the source term $\eta\boldsymbol{J}\cdot\boldsymbol{B}$.[27,28]

B. Resistive and advecto-resistive gauges

There are two important issues to be noted about the equations discussed above. First, for numerical reasons, Eq. (2) is often replaced by

$$\frac{\partial\boldsymbol{A}^r}{\partial t} = \boldsymbol{U}\times\boldsymbol{B} + \eta\nabla^2\boldsymbol{A}^r, \tag{11}$$

where $\boldsymbol{A}^r$ is the magnetic vector potential in the resistive gauge and we have assumed that η=const; otherwise there would be an additional gradient term of the magnetic diffusivity that results from[29]

$$-\eta\boldsymbol{J} + \boldsymbol{\nabla}(\eta\boldsymbol{\nabla}\cdot\boldsymbol{A}) = \eta\nabla^2\boldsymbol{A} + (\boldsymbol{\nabla}\cdot\boldsymbol{A})\,\boldsymbol{\nabla}\,\eta. \tag{12}$$

This "resistive" gauge introduces an explicit, numerically stabilizing diffusion term for each component of $\boldsymbol{A}$. Second, and again for numerical reasons, Eq. (5) should be solved with a small diffusion term proportional to $\nabla^2\Lambda^{W:a}$. These two issues are actually connected and can be resolved by considering the gauge transformation

$$\boldsymbol{A}^{\mathrm{ar}} = \boldsymbol{A}^r + \boldsymbol{\nabla}\Lambda^{r:\mathrm{ar}} \tag{13}$$

which allows us to obtain the magnetic vector potential $\boldsymbol{A}^{\mathrm{ar}}$ in the advecto-resistive gauge obeying

$$\frac{DA_i^{\mathrm{ar}}}{Dt} = -U_{j,i}A_j^{\mathrm{ar}} + \eta\nabla^2A_i^{\mathrm{ar}}, \tag{14}$$

by solving Eq. (11) for $\boldsymbol{A}^r$ together with

$$\frac{D\Lambda^{r:\mathrm{ar}}}{Dt} = -\boldsymbol{U}\cdot\boldsymbol{A}^r + \eta\nabla^2\Lambda^{r:\mathrm{ar}} \tag{15}$$

and finally using the gauge transformation Eq. (13). For a full derivation of this equation we refer to Appendix B. Note that the microscopic magnetic diffusivity automatically enters the $\Lambda^{r:\mathrm{ar}}$ equation as a diffusion term, which implies that the $\Lambda^{r:\mathrm{ar}}$ equation is numerically well behaved.

The magnetic helicity density $h^{\mathrm{ar}}=\boldsymbol{A}^{\mathrm{ar}}\cdot\boldsymbol{B}$ in the advecto-resistive gauge can be calculated from the magnetic helicity in the resistive gauge through $h^{\mathrm{ar}}=h^r+\boldsymbol{\nabla}\Lambda^{r:\mathrm{ar}}\cdot\boldsymbol{B}$, and it obeys

$$\frac{\partial h^{\mathrm{ar}}}{\partial t} = -2\eta\boldsymbol{J}\cdot\boldsymbol{B} - \boldsymbol{\nabla}\cdot\boldsymbol{F}^{\mathrm{ar}} \tag{16}$$

with

$$\boldsymbol{F}^{\mathrm{ar}} = h^{\mathrm{ar}}\boldsymbol{U} - \eta(\boldsymbol{\nabla}\cdot\boldsymbol{A}^{\mathrm{ar}})\boldsymbol{B} + \eta\boldsymbol{J}\times\boldsymbol{A}^{\mathrm{ar}}. \tag{17}$$

For comparison, the evolution equation of the magnetic helicity density in the resistive gauge is given by an equation similar to Eq. (16), but with h^{ar} being replaced by h^r and $\boldsymbol{F}^{\mathrm{ar}}$ being replaced by

$$\boldsymbol{F}^r = h^r\boldsymbol{U} - (\boldsymbol{U}\cdot\boldsymbol{A}^r + \eta\,\boldsymbol{\nabla}\cdot\boldsymbol{A}^r)\boldsymbol{B} + \eta\boldsymbol{J}\times\boldsymbol{A}^r \tag{18}$$

which contains a nonadvective velocity driven flux of the form $(\boldsymbol{U}\cdot\boldsymbol{A}^r)\boldsymbol{B}$—even in the ideal case.

C. Numerical details

We perform simulations for isotropically forced, triply periodic cubic domains with sides of length 2π, as was done in earlier work.[28] The $\eta\boldsymbol{J}\cdot\boldsymbol{B}$ term in Eq. (9) implies (and past simulations have shown) that such a system will experience a slow, but steady production of magnetic helicity. This is the price to pay for a system which is both helical, providing us with a signal, and homogeneous, so avoiding extraneous magnetic helicity fluxes. In addition to the uncurled induction Eq. (11) and the gauge transformation evolution Eq. (15), we solve

$$\frac{D\boldsymbol{U}}{Dt} = -c_s^2\,\boldsymbol{\nabla}\,\ln\rho + \frac{c_L}{\rho}\boldsymbol{J}\times\boldsymbol{B} + \boldsymbol{F}_{\mathrm{visc}} + \boldsymbol{f}, \tag{19}$$

$$\frac{D\ln\rho}{Dt} = -\boldsymbol{\nabla}\cdot\boldsymbol{U}, \tag{20}$$

where c_s(=const) is the isothermal sound speed, ρ is the density, $\boldsymbol{F}_{\mathrm{visc}}=\rho^{-1}\boldsymbol{\nabla}\cdot(2\rho\nu\mathsf{S})$ is the viscous force, $\mathsf{S}_{ij}=\frac{1}{2}(U_{i,j}+U_{j,i})-\frac{1}{3}\delta_{ij}\boldsymbol{\nabla}\cdot\boldsymbol{U}$ is the rate of strain tensor, ν is the kinematic viscosity, $\boldsymbol{f}$ the forcing term, and $c_L=1$ is a prefactor that can be put to 0 to turn off the Lorentz force in kinematic calculations. As in earlier work[28] the forcing function consists of plane polarized waves whose direction and phase change randomly from one time step to the next. The modulus of its wavevectors is taken from a band of wavenumbers around a given average wavenumber k_f. The magnetic vector potential is initialized with a weak nonhelical sine wave

along one direction. In some cases we shall also consider solutions to the passive scalar equation in the incompressible case

$$\frac{DC}{Dt} = \kappa \nabla^2 C, \tag{21}$$

where κ is the passive scalar diffusivity. Following earlier work,[30] we impose a linear gradient in C, i.e., $C=Gz+c$, and solve for the departure from this gradient G, i.e.,

$$\frac{Dc}{Dt} = \kappa \nabla^2 c - GU_z, \tag{22}$$

where GU_z acts essentially as a forcing term.

We use the PENCIL CODE (http://pencil-code.googlecode.com)[31] to solve the equations for $\boldsymbol{A}^r$, $\boldsymbol{U}$, $\Lambda^{r:\mathrm{ar}}$, ρ, and in some cases also c. The calculations involving $\Lambda^{r:\mathrm{ar}}$ have been carried out with the publicly available revision r15211 (or similar) of the module special/advective_gauge.f90.

The control parameters we use are the magnetic Reynolds number Re_M, the magnetic Prandtl number Pr_M, and the Schmidt number

$$\mathrm{Re}_M \equiv \frac{u_{\mathrm{rms}}}{\eta k_f}, \quad \mathrm{Pr}_M \equiv \frac{\nu}{\eta}, \quad \mathrm{Sc} \equiv \frac{\nu}{\kappa}, \tag{23}$$

where u_{rms} is the root mean square velocity. We use $k_f=3k_1$ where k_1, the box wavenumber, is unity. The numerical resolution is varied between 32^3 and 256^3 meshpoints for values of Re and Re_M between 3 and 300. In one case we used $\mathrm{Re}_M \approx 800$, which was only possible because in that case we used $\mathrm{Pr}_M=10$, so that most of the energy gets dissipated viscously, leaving relatively little magnetic energy at high wavenumbers.[32]

III. IMPORTANCE OF MAGNETIC HELICITY DENSITY

A. Implications of Eq. (7) for dynamo theory

Magnetic helicity is not only of interest by being a conserved quantity in ideal MHD, but also by being the basis of a methodology to treat nonlinear helical MHD dynamos, namely, dynamical α quenching.[33] This methodology relates the current helicity in small scale fields with the magnetic helicity in small-scale fields, $\boldsymbol{j}\cdot\boldsymbol{b} \simeq k_f^2 \boldsymbol{a}\cdot\boldsymbol{b}$, and invokes the magnetic α effect.[4] The evolution equation of the magnetic helicity density then becomes the evolution equation of the magnetic part of the α effect and the nonlinear evolution of the dynamo can be modeled. This methodology has been used successfully in systems where no net helicity flux is possible, and initial work invoking the methodology has captured the behavior of at least one system with finite helicity fluxes.[34] A major prediction of the theory is that in the absence of preferential helicity fluxes of small-scale fields, dynamo action is quenched to subequipartition mean field strengths. This phenomenon is sometimes referred to as "catastrophic quenching."

B. Magnetic helicity as passive scalar

In the advective and advecto-resistive gauges, the velocity appears in the evolution equations of the magnetic helicity density, Eqs. (7) and (16), only as advection terms in the fluxes, Eqs. (10) and (17). In the limit of ideal, incompressible, kinematic MHD, Eq. (7) is the evolution equation for a passive scalar. Even in nonideal MHD, if the fluctuations of h^{ar} due to the velocity field $\boldsymbol{U}$ were purely advective in nature (i.e., passive), magnetic helicity transport would only be resistive, large-scale advective, and/or turbulently diffusive. This would forbid the preferential export of small-scale magnetic helicity and might call for alternate solutions to the catastrophic quenching problem than helicity fluxes.[18]

While in ideal MHD ($\eta=0$) the resistive terms in Eq. (7) vanish, resistive terms need not vanish in the limit of $\eta \to 0$ (high Re_M). For example, in a turbulent flow, Ohmic dissipation $\eta \boldsymbol{J}^2$ tends to a finite value as η decreases. The need for nonresistive solutions to the build-up of magnetic helicity is therefore not a given. We will examine this by performing kinematic simulations where the Lorentz force is turned off, i.e., $c_L=0$.

If the Lorentz force is significant, the fluctuations of h^{ar} and $\boldsymbol{U}$ might be correlated beyond simple turbulent diffusion concerns (i.e., the fluctuations of h^{ar} could drive flow patterns). In the limit of incompressible flows, if the helicity is uniform, then the only source terms for helicity patterns of finite k are the resistive terms. The terms are small compared to dimensional estimates for the velocity terms when $\mathrm{Re}_M \gg 1$. We will look for signals of magnetic helicity transport by examining spectra of h^r and h^{ar} as (pseudo) scalars, together with spectra of a true passive scalar. As we will show, the advecto-resistive gauge is adequately efficient at turbulently diffusing magnetic helicity that no inertial range for the magnetic helicity density can be identified. However, the spectra of h^r help elucidate previous results[34] which found diffusive fluxes, but at values well below turbulent diffusivities. Instead, our spectra show clear diffusive behavior in the inertial range, but the mere existence of the inertial range implies nondiffusive behavior.

We emphasize that our spectra of h^r and h^{ar} have nothing to do with the usual magnetic helicity spectrum that obeys a realizability condition and whose integral gives the volume-averaged magnetic helicity. Here we are looking instead at the power of the magnetic helicity density as a (pseudo) scalar field. Our h_k measures the spatial variation of h. In order to avoid confusion, we shall refer to these spectra as scalar spectra.

IV. RESULTS

The results reported below for the magnetic helicity density h refer to the advecto-resistive gauge and have been obtained by the Λ method, unless indicated otherwise. The results from the direct method agree (Sec. IV A), but this method develops an instability when nonlinear effects become important (Sec. IV B).

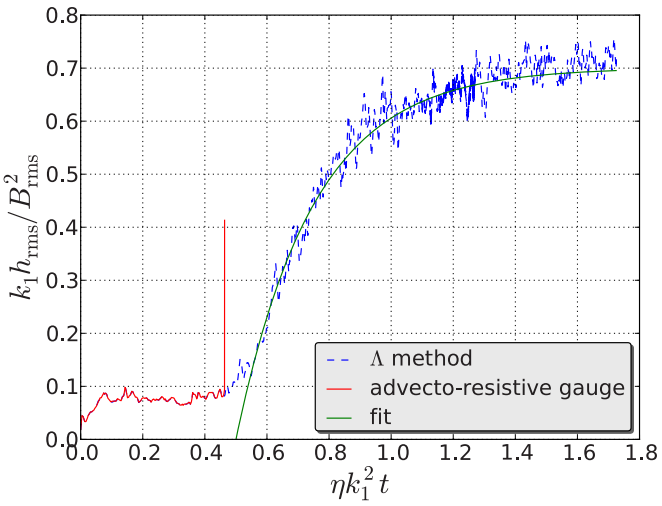

FIG. 1. (Color online) Time dependence of the normalized helicity for the advecto-resistive gauge with the direct method and the Λ method. Both curves agree perfectly just until the moment when the code develops an instability in the direct calculation. Time is normalized in terms of the magnetic diffusion time. The fit is an exponential relaxation to a constant value proportional to $1-\exp(-2\eta k_m^2 \Delta t)$, where $\Delta t = t - t_{\rm sat}$ is the time after the small-scale magnetic field has saturated (Ref. 28) and $k_m = 1.4 k_1$ has been chosen for a good fit.

A. Agreement between Λ and direct methods

To test the agreement between the Λ method and directly solving the induction equation in the advecto-resistive gauge, we plot the normalized rms magnetic helicity $h_{\rm rms}^{\rm ar}$ with respect to time (Fig. 1). Note that the nondimensional ratio $k_1 h_{\rm rms}^{\rm ar}/B_{\rm rms}^2$ has a well-defined plateau during the kinematic stage. Below we shall study the average value of this plateau as a function of magnetic Reynolds and Prandtl numbers. At the end of the kinematic phase, there is a slow saturation phase on a resistive time scale during which the large-scale field of the dynamo develops.[28] The results of the two calculations agree just until the moment when the direct calculation develops a numerical instability, whose nature will be discussed in more detail below. The perfect agreement until this moment can be taken as confirmation that the Λ method works and is correctly implemented in the code.

B. Nature of the instability

In Fig. 2 we show time series for a range of modest values of Re_M and two resolutions, 32^3 and 64^3. Reducing the magnetic Reynolds number may stabilize the system somewhat, but changing the resolution has no clear effect. In Fig. 3 we present data from equivalent runs that solve either Eq. (14) or alternatively Eqs. (11) and (15). We can see that the solutions match up until time $t = 220/c_s k_f$, where the run that solves Eq. (14) becomes unstable.

The key point is that when we evolve Eqs. (11) and (15), Λ never enters the equations for physical quantities. However, when we evolve Eq. (14), the magnetic field includes a term $\boldsymbol{\nabla}\times(\boldsymbol{\nabla}\Lambda)$, which, when computed numerically, is not zero. The first panel in Fig. 3 shows the power spectra of the vector potential. Comparing the advecto-resistive gauge (dashed/red) with resistive gauge (dotted/blue) we see that

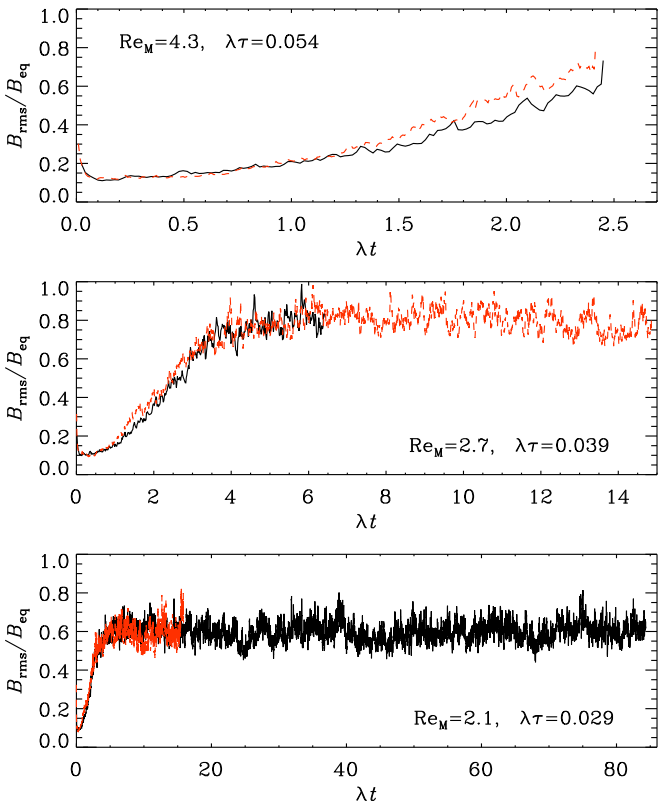

FIG. 2. (Color online) Evolution of $B_{\rm rms}/B_{\rm eq}$ for small values of Re_M between 4.3 (top) and 2.1 (bottom), using 32^3 (solid lines) and 64^3 (dashed, red lines). In each case, time on the abscissa is normalized by the growth rate λ, whose value is given in each panel in units of the inverse turnover time, $\tau^{-1} = u_{\rm rms} k_f$. The ends of each line mark the point when the solution became unstable.

$\boldsymbol{A}^{\rm ar} = \boldsymbol{A}^r + \boldsymbol{\nabla}\Lambda$ has significantly more power at high k than $\boldsymbol{A}^r$. Numerics cannot adequately handle the requirement that $\boldsymbol{\nabla}\times\boldsymbol{\nabla}\Lambda = 0$ at high k in the direct method, introducing errors in $\boldsymbol{B}$, as can be seen in the second panel. This fictitious increase in magnetic power at high k (and the attendant increase in current) result in a fictitious high k increase in the velocity field (third panel) that produces the numerical instability. The results of Fig. 2 suggest that the power of Λ (remembering that $\boldsymbol{J}$ includes that the third derivative of Λ) drops slowly enough at high k that numerical stability can only be achieved by enforcing an adequate resistivity η to damp Λ for only modest wavenumbers. Indeed, any gauge with large power in $\boldsymbol{A}$ for high k is expected to be numerically unstable, and the method sketched in Appendix A orAppendix B may be used to make the connection between analytical results in such a numerically unstable gauge and numerical results produced in a stable gauge.

C. Evolution of rms helicity density

In Fig. 4 we present a time series of the normalized rms magnetic helicity density in the kinematic regime (Lorentz force turned off, i.e., $c_L = 0$). In both the advecto-resistive and resistive gauges, there is an initial adjustment of the nondimensional ratio $k_1 h_{\rm rms}/B_{\rm rms}^2$ to a certain value, followed by a plateau. In the kinematic regime the magnetic helicity

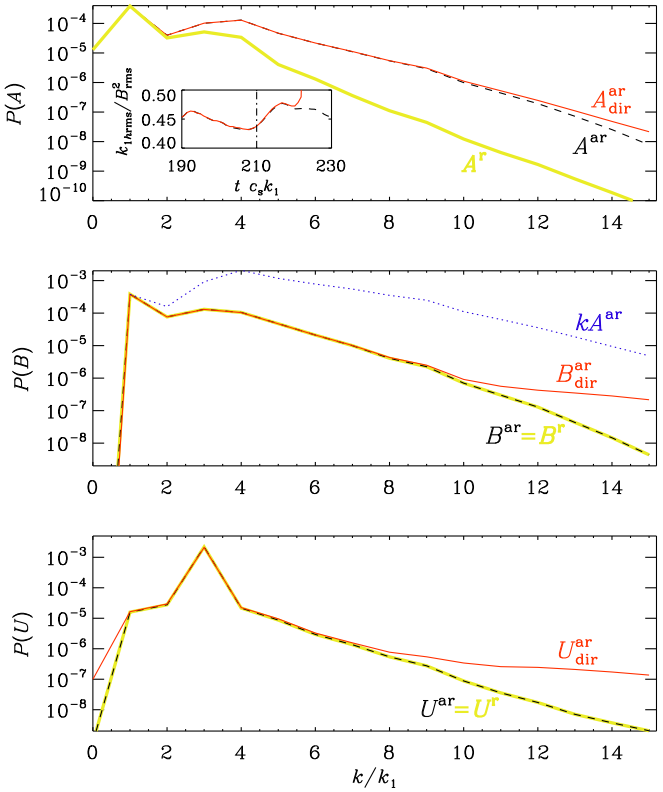

FIG. 3. (Color online) Power spectra of $\boldsymbol{A}$, $\boldsymbol{B}$, and $\boldsymbol{U}$ for two runs that are identical except that the first run solves for $\boldsymbol{A}^{\rm ar}$ directly while the second solves for $\boldsymbol{A}^r$ and Λ. In the top panel we plot the spectrum of $\boldsymbol{A}$ obtained either via $\boldsymbol{A}^{\rm ar}=\boldsymbol{A}^r+\boldsymbol{\nabla}\Lambda$ (dashed) or directly, $\boldsymbol{A}^{\rm ar}_{\rm dir}$ (solid/red), and compare with $\boldsymbol{A}^r$ (thick gray/yellow), showing that the vector potential in the advecto-resistive gauge has much more power at high k. The inset shows the time evolution of the normalized $h_{\rm rms}$ shortly before the time of the numerical instability. The dash-dotted line indicates the time for which the power spectra is taken. In the second panel we present magnetic energy spectra obtained in the direct gauge (solid/red), with the Λ method (dashed/black) as well as $k\boldsymbol{A}^{\rm ar}$ (dotted/blue), showing that there is significant power in the irrotational part of $\boldsymbol{A}$. We see that in the direct calculation of $\boldsymbol{A}^{\rm ar}$ the numerics are unable to adequately handle the high wavenumber power of $\boldsymbol{A}^{\rm ar}$ with consequences for the velocity seen in the last panel (solid/red line). The spectra of $\boldsymbol{B}$ and $\boldsymbol{U}$ agree for resistive and advecto-resistive gauges (thick gray/yellow line underneath the dashed black line) because the evaluation of the curl of a gradient has been avoided (last two panels). The three spectra are all taken for $t=210/c_s k_1$.

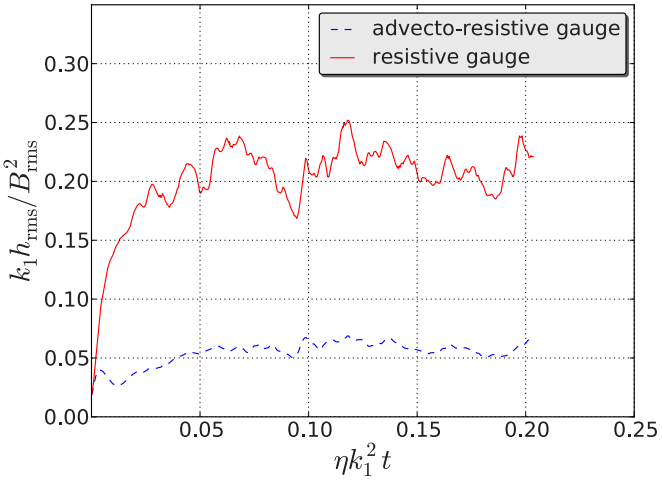

FIG. 4. (Color online) Time dependence of the rms values for the helicity in the advecto-resistive (solid/red) and resistive (dashed/blue) gauges with the Lorentz force switched off, i.e., $c_L=0$ in both cases.

density is passive and the advection term in the advecto-resistive gauge merely serves to turbulently diffuse any local concentrations of $h^{\rm ar}$. Therefore there cannot be any spontaneous growth of $h^{\rm ar}$, except for effects from the resistive terms in the early adjustment phase. Turbulent diffusion itself, on the other hand, cannot generate variance of $h^{\rm ar}$.

In Figs. 5 and 6 we plot the height of the rms-magnetic helicity density plateau as a function of Re_M for several values of the magnetic Prandtl number and constant forcing amplitude. The differences between the evolution equations for h^r and $h^{\rm ar}$ are contained entirely in the flux terms so the volume integral of h is the same in the two gauges. Any difference between the rms values of h therefore is due to spatial fluctuations generated by the flux terms.

We fit the data points in Fig. 5 with functions of the form

$$\frac{k_1 h^{\rm ar}}{B^2_{\rm rms}} = c\mathrm{Re}_M^{-a}(1+b\mathrm{Re}_M^{2a}). \tag{24}$$

The fit results for the parameters are presented in Table I. Of interest is c, which increases with Pr_M and scales approximately with $\mathrm{Pr}_M^{1/2}$. A more general, although less accurate fit is given by

$$\frac{k_1 h^{\rm ar}}{B^2_{\rm rms}} \approx 3\mathrm{Re}_M^{-1}\left[1+\left(\frac{\mathrm{Re}_M/\mathrm{Pr}_M^{1/3}}{50}\right)^2\right] \tag{25}$$

see Fig. 7.

It is clear that high wavenumber fluid eddies (which are damped for small Re, i.e., large Pr_M, contribute significantly to $h^{\rm ar}_{\rm rms}$ for $\mathrm{Re}_M>100$, while from Fig. 6 we see that they do not contribute to $h^r_{\rm rms}$. That these eddies could contribute in the advecto-resistive gauge is to be expected as the advective

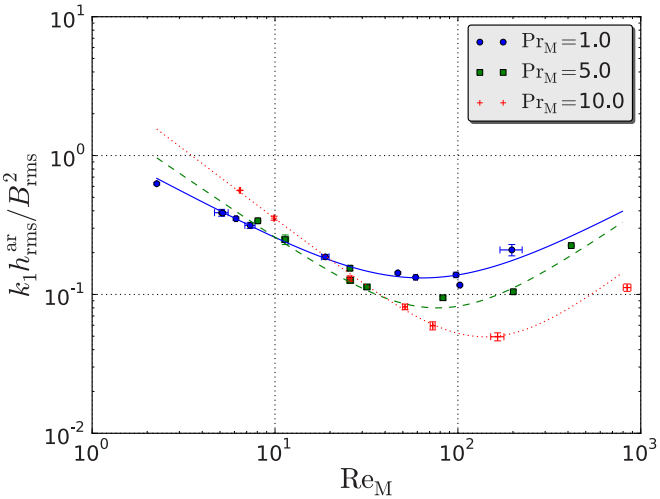

FIG. 5. (Color online) Re_M dependence of $k_1 h^{\rm ar}_{\rm rms}/B^2_{\rm rms}$ for the kinematic phase. Values are averages over times where they reach a stationary state. The curves represent fits according to Eq. (24).

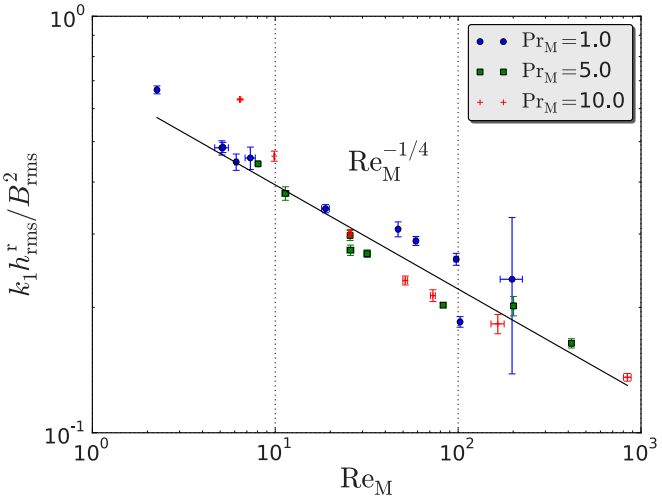

FIG. 6. (Color online) Re_M dependence of $k_1 h^r_{\rm rms}/B^2_{\rm rms}$ for the kinematic phase. Values are averages over times where they reach a stationary state. A $-1/4$ power law can be seen.

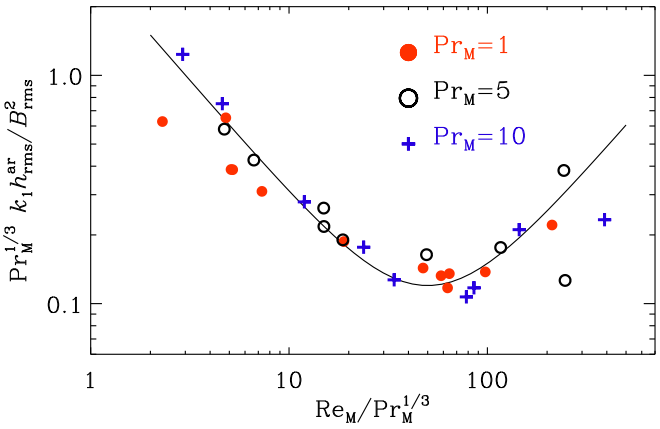

FIG. 7. (Color online) Dependence of $k_1 h^{\rm ar}_{\rm rms}/B^2_{\rm rms}$, scaled by $\mathrm{Pr}_M^{1/3}$ on $\mathrm{Re}_M/\mathrm{Pr}_M^{1/3}$ for the kinematic phase and $\mathrm{Pr}_M=1$ (filled circles), 5 (open circles), and 10 (plus signs). The solid line represents the fit of Eq. (25).

nature of that gauge implies the existence of an efficient turbulent cascade; the fact that they do contribute there and that the $\eta \boldsymbol{J}\times\boldsymbol{A}^{\rm ar}$ and $\eta(\boldsymbol{\nabla}\cdot\boldsymbol{A}^{\rm ar})\boldsymbol{B}$ terms remain important implies that resistive terms both become important at small length scales and have nondissipative effects. This is explained by the fact that $\boldsymbol{A}^{\rm ar}$ develops a strong high-k tail; see also Fig. 3. This is confirmed in Fig. 8, which shows that the resistive magnetic helicity fluxes in the advecto-resistive gauge are proportional to Re_M. In this gauge the rms resistive helicity fluxes are therefore independent of the actual value of the resistivity, staying finite even in the high Re_M limit. This is quite different from the resistive magnetic helicity fluxes in the resistive gauge, and the global magnetic helicity dissipation (which is gauge-independent): both terms are only proportional to $\mathrm{Re}_M^{1/2}$ and, after multiplying with η these terms tend to zero for $\mathrm{Re}_M\to\infty$.

D. Comparison with passive scalar

In Fig. 9 we present scalar spectra of the magnetic helicity density for both the resistive and advecto-resistive gauges and for the passive scalar concentration c, in the kinematic (arbitrary units) and saturated regimes. The passive scalar spectrum shows a peak at the forcing scale, $k_f/k_1=3$, followed by an approximate $k^{-5/3}$ subrange and an exponential diffusive subrange. As long as the magnetic energy density is still small compared with the kinetic energy density, the field exhibits exponential growth and a Kazantsev $k^{3/2}$ energy spectrum, which is well seen in simulations even at magnetic Prandtl numbers of unity both with and without kinetic helicity in the velocity field.[35] This $k^{3/2}$ spectrum is also reflected in the scalar spectrum of $h^{\rm ar}$. The scalar spectrum of h^r is somewhat steeper and closer to k^2, indicating that h^r is dominated by white noise in space at large scales.

The saturated regime exhibits some interesting properties. The pronounced peak of the power of the passive scalar at the driving scale is easily understood as being due to the source of c. However, the magnetic helicity density in the resistive gauge shows a significant peak there as well, while it does not in the advecto-resistive gauge. This implies that the velocity term in Eq. (18) generates significant spatial variations in the magnetic helicity density—even in the absence of external modulations. As in dynamical α quenching, h influences the α effect, this suggests a way to quantify the appropriateness of different gauge choices: systems where spatial and temporal fluctuations in α can be adequately constrained would allow one to determine whether spatial fluctuations in h, as seen in Fig. 9, are fictitious as suggested by the advecto-resistive gauge or not.

TABLE I. Fit parameters for Eq. (24) and Fig. 5.

Pr_M	a	b	c	Line type
1	0.7	3×10^{-3}	1.2	Solid/blue
5	0.9	4×10^{-4}	2.0	Dashed/green
10	1.0	5×10^{-5}	3.5	Dotted/red

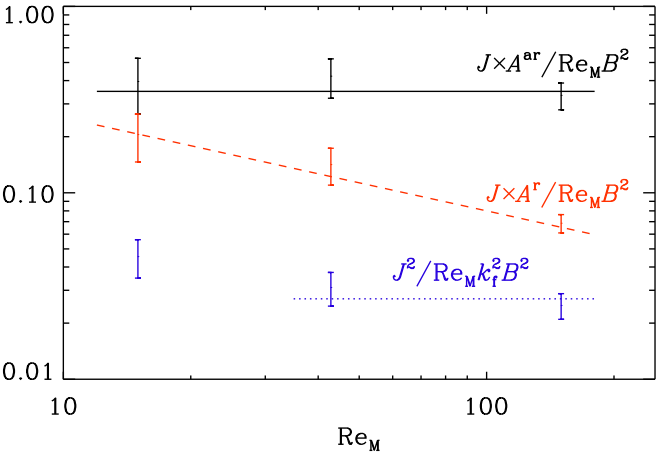

FIG. 8. (Color online) Re_M scaling of the rms value of $\boldsymbol{J}\times\boldsymbol{A}$, normalized by $\mathrm{Re}_M B^2_{\rm rms}$, for the advecto-resistive and resistive gauges. The solid line represents constant scaling, i.e., $\eta\boldsymbol{J}\times\boldsymbol{A}^{\rm ar}\approx$const, while the dashed line represents inverse square root scaling, i.e., $\eta\boldsymbol{J}\times\boldsymbol{A}^{r}\propto\mathrm{Re}_M^{-1/2}$, for three runs with $\mathrm{Pr}_M=1$ in the saturated regime. The dotted/blue line shows that ηJ^2, properly normalized, is approximately constant.

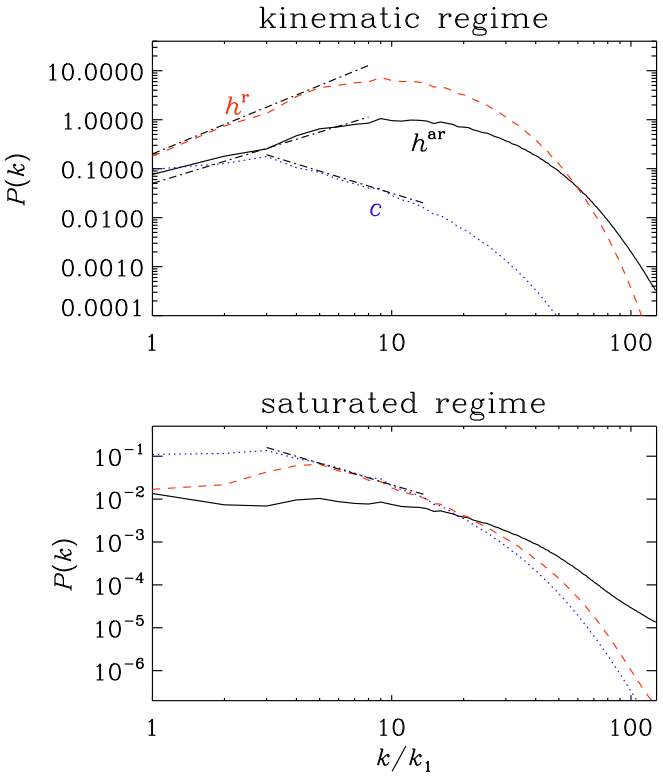

FIG. 9. (Color online) Power spectra of h^r, h^{ar}, and the passive scalar c, both in the kinematic regime (top) and the nonlinear saturated regime (bottom) for Re=80 with $\mathrm{Pr}_M=\mathrm{Sc}=1$. In the kinematic regime, the dash-dotted lines have slopes +2 for h^r, +3/2 for h^{ar}, −3/2 for c (top), and −5/3 for c in the saturated regime.

The spectra of h^{ar} in the saturated regime do not present a clear inertial range, so we cannot draw strong conclusions as to possible nondiffusive turbulent fluxes. However, h^r follows the same cascade as the passive scalar. Previous studies in that gauge[1] found that magnetic helicity fluxes were best treated as diffusive, although the fits were imperfect. The diffusive nature is clearly seen in the spectrum while the imperfections of the diffusive fit can be seen in the generation of a peak at the driving scale. This evidence in support of diffusive magnetic helicity fluxes gives us the confidence to predict at what Re_M diffusive magnetic helicity fluxes will play a dominant role in dynamo saturation, i.e., when the diffusive fluxes have a greater effect on magnetic helicity evolution than the resistive terms. This will be done in Sec. V where we reanalyze simulation data from earlier work.[34]

V. REVISITING EARLIER WORK

Earlier work[20,34] on magnetic helicity fluxes in inhomogeneous open systems confirmed that the magnetic helicity density of the small-scale field is gauge-invariant —even if that of the large-scale field is not. The divergence of the mean magnetic helicity flux of the small-scale field is then also gauge-invariant, but its value is small compared with resistive magnetic helicity dissipation. We return to this work to estimate at what Re_M diffusive magnetic helicity fluxes will begin to play a dominant role in dynamo saturation.

We emphasize that we are now discussing helicity properties of what we call the small-scale field. Such a field is

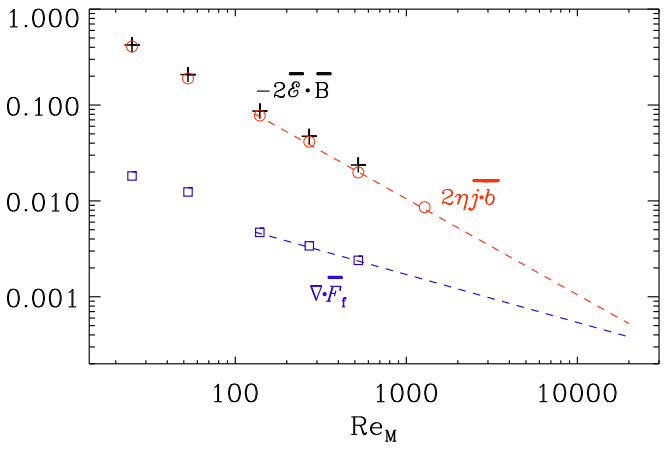

FIG. 10. (Color online) Scaling of $\bar{\mathcal{E}}\cdot\bar{\boldsymbol{B}}$, $\overline{\boldsymbol{j}\cdot\boldsymbol{b}}$, and $\boldsymbol{\nabla}\cdot\bar{\boldsymbol{F}}_f$ vs Re_M for the data of an earlier simulation (Ref. 34) of helically driven turbulence embedded in a poorly conducting nonhelically driven turbulent halo. The symbols show actual data obtained from simulations, the dashed lines are the extrapolation to high Re_M.

defined by introducing an averaged magnetic field, $\bar{\boldsymbol{B}}$, indicated by an overbar. Following earlier work[20,34] we restrict ourselves here to planar (or horizontal) averaging. The small-scale field is then given by $\boldsymbol{b}=\boldsymbol{B}-\bar{\boldsymbol{B}}$, and the mean magnetic and current helicity densities of the fluctuating fields are then $\bar{h}_f\equiv\overline{\boldsymbol{a}\cdot\boldsymbol{b}}$ and $\overline{\boldsymbol{j}\cdot\boldsymbol{b}}$, respectively, where $\boldsymbol{\nabla}\times\boldsymbol{a}=\boldsymbol{b}$ and $\boldsymbol{j}=\boldsymbol{\nabla}\times\boldsymbol{b}$. Turbulent diffusion and the α effect imply helicity transfer between scales[36,37] through the mean electromotive force of the fluctuating field, $\bar{\mathcal{E}}=\overline{\boldsymbol{u}\times\boldsymbol{b}}$, so that the evolution equation for $\bar{h}_f$ takes the form

$$\frac{\partial\bar{h}_f}{\partial t}=-2\bar{\mathcal{E}}\cdot\bar{\boldsymbol{B}}-2\eta\overline{\boldsymbol{j}\cdot\boldsymbol{b}}-\boldsymbol{\nabla}\cdot\bar{\boldsymbol{F}}_f. \tag{26}$$

Here, both $\bar{h}_f$ and $\boldsymbol{\nabla}\cdot\bar{\boldsymbol{F}}_f$ are a gauge-dependent, but if there is a steady state, and if $\bar{h}_f$ is constant, then $\partial\bar{h}_f/\partial t=0$, and since both $\bar{\mathcal{E}}\cdot\bar{\boldsymbol{B}}$ and $\overline{\boldsymbol{j}\cdot\boldsymbol{b}}$ are gauge-invariant, $\boldsymbol{\nabla}\cdot\bar{\boldsymbol{F}}_f$ must also be gauge-invariant. Numerical values for $\bar{\mathcal{E}}\cdot\bar{\boldsymbol{B}}$, $\overline{\boldsymbol{j}\cdot\boldsymbol{b}}$, and $\boldsymbol{\nabla}\cdot\bar{\boldsymbol{F}}_f$ were given earlier[34] for a particular simulation of a slab of helically driven turbulence embedded in a poorly conducting nonhelically driven turbulent halo. In Fig. 10 we show the scaling of all three terms versus Re_M. Note that $-\bar{\mathcal{E}}\cdot\bar{\boldsymbol{B}}$ is balanced mainly by $\overline{\boldsymbol{j}\cdot\boldsymbol{b}}$. However, if the current trend, $\overline{\boldsymbol{j}\cdot\boldsymbol{b}}\sim\mathrm{Re}_M^{-1}$ and $\boldsymbol{\nabla}\cdot\bar{\boldsymbol{F}}_f\sim\mathrm{Re}_M^{-1/2}$ were to continue, one might expect a cross-over at $\mathrm{Re}_M\approx3\times10^4$. If so, the scaling of $\bar{\mathcal{E}}\cdot\bar{\boldsymbol{B}}$ is expected to become shallower, following that of $\boldsymbol{\nabla}\cdot\bar{\boldsymbol{F}}_f$. Given that the largest Re_M accessible today is of order 10^3, we may conclude that an alleviation of quenching through diffusive magnetic helicity fluxes will not be prominent in simulations for the near future. Nevertheless, astrophysical systems such as the Sun are orders of magnitude beyond the estimated critical point of $\mathrm{Re}_M\sim3\times10^4$; and we expect their dynamo dynamics to behave accordingly.

VI. CONCLUSIONS

In view of the fact that the time averaged magnetic helicity of the fluctuating fields is gauge-invariant in systems with sufficient scale separation, the gauge-freedom can be exploited to gain insights using gauges that are particularly revealing. Here we have examined an interesting gauge: the advecto-resistive gauge. As the advecto-resistive gauge is inherently numerically unstable, we had to implement a possibly universal technique to run numerical simulations in such unstable gauges by running in a stable gauge while also solving a further equation for the gauge transformation.

The advecto-resistive gauge has allowed us to examine both the consequences of finite resistivity for magnetic helicity density as well as the possibilities of turbulent transport. The magnetic helicity flux, and in particular the contribution from $\eta \boldsymbol{J}\times\boldsymbol{A}^{\rm ar}$ (properly normalized) reaches a constant value as $\eta\to 0$. This behavior is similar to the behavior of energy dissipation in turbulence, known as the law of finite energy dissipation.[38] This is interesting as the source term for the volume integrated magnetic helicity H does in fact tend to zero as η does. In this sense, the high Re_M behavior of magnetic helicity is richer than previously anticipated. Indeed, the generation of spatial magnetic helicity fluctuations *ex nihilo* in nonadvecto-resistive gauges is interesting, with potentially testable implications. We expect that the magnetic helicity fluxes resulting from terms of the form $\eta \boldsymbol{J}\times\boldsymbol{A}^{\rm ar}$ can be modeled as turbulent Fickian diffusion-type fluxes down the gradient of mean magnetic helicity. However, it is clear that fluxes from turbulent diffusion provide only a poor escape from catastrophic α quenching, partly because they cannot distinguish between large- and small-scale fields. Furthermore, in simulations with such turbulent diffusion fluxes, their contribution is still much smaller than the local resistive magnetic helicity dissipation.[20,34] However, the latter decreases faster ($\sim \mathrm{Re}_M^{-1}$) with magnetic Reynolds number than the former ($\sim \mathrm{Re}_M^{-1/2}$), so one may estimate that only for magnetic Reynolds numbers of around 10^4 one has a chance to see the effects of turbulent diffusion. If true, however, such fluxes would definitely be important for the magnetic Reynolds numbers relevant to stars and galaxies—even though such values cannot be reached with present day computer power.

ACKNOWLEDGMENTS

National Supercomputer Centre in Linköping and the Center for Parallel Computers at the Royal Institute of Technology in Sweden. This work was supported in part by the Swedish Research Council (Grant No. 621-2007-4064), and the European Research Council under the AstroDyn Research Project 227952.

APPENDIX A: DERIVATION OF EQ. (5)

We begin by expressing $\boldsymbol{U}\times\boldsymbol{B}$ in terms of $\boldsymbol{A}$

$$(\boldsymbol{U}\times\boldsymbol{B})_i = U_j A_{j,i} - U_j A_{i,j}. \tag{A1}$$

The last term can be subsumed into an advective derivative term for $\boldsymbol{A}$. Using furthermore $U_j A_{j,i} = (U_j A_j)_{,i} - U_{j,i} A_j$, we can write Eq. (2) as

$$\frac{DA_i^W}{Dt} = -U_{j,i}A_j^W + (\boldsymbol{U}\cdot\boldsymbol{A}^W)_{,i} - \eta J_i. \tag{A2}$$

We now insert Eq. (3) for $\boldsymbol{A}^W = \boldsymbol{A}^a - \boldsymbol{\nabla}\Lambda^{W:a}$, so

$$\frac{DA_i^a}{Dt} - \frac{D\Lambda_{,i}^{W:a}}{Dt} = -U_{j,i}A_j^a + U_{j,i}\Lambda_{,j}^{W:a} + (\boldsymbol{U}\cdot\boldsymbol{A}^W)_{,i} - \eta J_i. \tag{A3}$$

and note that

$$-\frac{D\Lambda_{,i}^{W:a}}{Dt} = -\nabla_i\left(\frac{D\Lambda^{W:a}}{Dt}\right) + U_{j,i}\Lambda_{,j}^{W:a}. \tag{A4}$$

The last term cancels and we are left with

$$\frac{DA_i^a}{Dt} + U_{j,i}A_j^a + \eta J_i = \nabla_i\left(\frac{D\Lambda^{W:a}}{Dt} + \boldsymbol{U}\cdot\boldsymbol{A}^W\right), \tag{A5}$$

so we recover the evolution equation for the advective gauge provided Eq. (5) is obeyed.

APPENDIX B: DERIVATION OF EQ. (15)

We present here the derivation of the transformation from the resistive gauge to the advecto-resistive gauge, proceeding analogously to the derivation presented in Appendix A. However, instead of Eq. (A2) we now have

$$\frac{DA_i^r}{Dt} = -U_{j,i}A_j^r + (\boldsymbol{U}\cdot\boldsymbol{A}^r)_{,i} + \eta\nabla^2 A_i^r. \tag{B1}$$

Inserting Eq. (13) for $\boldsymbol{A}^r = \boldsymbol{A}^{\rm ar} - \boldsymbol{\nabla}\Lambda^{r:{\rm ar}}$, we obtain an Equation similar to Eq. (A3)

$$\frac{DA_i^{\rm ar}}{Dt} - \frac{D\Lambda_{,i}^{r:{\rm ar}}}{Dt} = -U_{j,i}A_j^{\rm ar} + U_{j,i}\Lambda_{,j}^{r:{\rm ar}} + (\boldsymbol{U}\cdot\boldsymbol{A}^r)_{,i} + \eta\nabla^2 A_i^{\rm ar} - \eta\nabla^2\Lambda_{,i}^{r:{\rm ar}} \tag{B2}$$

which leads to

$$\frac{DA_i^{\rm ar}}{Dt} + U_{j,i}A_j^{\rm ar} - \eta\nabla^2 A_i^{\rm ar} = \nabla_i\left(\frac{D\Lambda_i^{r:{\rm ar}}}{Dt} + \boldsymbol{U}\cdot\boldsymbol{A}^r - \eta\nabla^2\Lambda^{r:{\rm ar}}\right) \tag{B3}$$

so we recover the evolution equation for the advecto-resistive gauge provided Eq. (15) is obeyed.

[1] A. Hubbard and A. Brandenburg, Astrophys. J. **727**, 11 (2010).
[2] J. B. Taylor, Rev. Mod. Phys. **58**, 741 (1986).
[3] W. H. Matthaeus and D. Montgomery, Ann. N.Y. Acad. Sci. **357**, 203 (1980).
[4] A. Pouquet, U. Frisch, and J. Leorat, J. Fluid Mech. **77**, 321 (1976).
[5] A. Brandenburg and K. Subramanian, Phys. Rep. **417**, 1 (2005).
[6] S. I. Vainshtein and F. Cattaneo, Astrophys. J. **393**, 165 (1992).
[7] F. Cattaneo and D. W. Hughes, Phys. Rev. E **54**, R4532 (1996).

[8]E. G. Blackman and G. B. Field, Mon. Not. R. Astron. Soc. **318**, 724 (2000).
[9]E. G. Blackman and G. B. Field, Astrophys. J. **534**, 984 (2000).
[10]B. P. Brown, M. K. Browning, A. S. Brun, M. S. Miesch, and J. Toomre, Astrophys. J. **711**, 424 (2010).
[11]P. J. Käpylä, M. J. Korpi, A. Brandenburg, D. Mitra, and R. Tavakol, Astron. Nachr. **331**, 73 (2010).
[12]P. Charbonneau, Living Reviews in Solar Physics **7**, 3 (2010), http://livingreviews.org/lrsp-2010-3.
[13]S. E. Gibson, L. Fletcher, G. D. Zanna, C. D. Pike, H. E. Mason, C. H. Mandrini, P. Dmoulin, H. Gilbert, J. Burkepile, T. Holzer, D. Alexander, Y. Liu, N. Nitta, J. Qiu, B. Schmieder, and B. J. Thompson, Astrophys. J. **574**, 1021 (2002).
[14]K. D. Leka, R. C. Canfield, A. N. McClymont, and L. van Driel-Gesztelyi, Astrophys. J. **462**, 547 (1996).
[15]P. K. Manoharan, L. van Driel-Gesztelyi, M. Pick, and P. Demoulin, Astrophys. J. **468**, L73+ (1996).
[16]R. C. Canfield, H. S. Hudson, and D. E. McKenzie, Geophys. Res. Lett. **26**, 627, doi:10.1029/1999GL900105 (1999).
[17]A. Shukurov, D. Sokoloff, K. Subramanian, and A. Brandenburg, Astron. Astrophys. **448**, L33 (2006).
[18]A. Brandenburg, S. Candelaresi, and P. Chatterjee, Mon. Not. R. Astron. Soc. **398**, 1414 (2009).
[19]E. G. Blackman and A. Brandenburg, Astrophys. J. **584**, L99 (2003).
[20]D. Mitra, S. Candelaresi, P. Chatterjee, R. Tavakol, and A. Brandenburg, Astron. Nachr. **331**, 130 (2010).
[21]K. Subramanian and A. Brandenburg, Astrophys. J. Lett. **648**, L71 (2006).
[22]E. T. Vishniac and J. Cho, Astrophys. J. **550**, 752 (2001).
[23]D. J. Price and C. Federrath, Astron. Soc. Pac. Conf. Ser. **429**, 274 (2010).
[24]D. J. Price, Mon. Not. R. Astron. Soc. **401**, 1475 (2010).
[25]A. Brandenburg, Mon. Not. R. Astron. Soc. **401**, 347 (2010).
[26]A. Brandenburg, A. Nordlund, R. F. Stein, and U. Torkelsson, Astrophys. J. **446**, 741 (1995).
[27]M. A. Berger, Geophys. Astrophys. Fluid Dyn. **30**, 79 (1984).
[28]A. Brandenburg, Astrophys. J. **550**, 824 (2001).
[29]W. Dobler, A. Shukurov, and A. Brandenburg, Phys. Rev. E **65**, 036311 (2002).
[30]A. Brandenburg, P. J. Käpylä, and A. Mohammed, Phys. Fluids **16**, 1020 (2004).
[31]A. Brandenburg and W. Dobler, Comput. Phys. Commun. **147**, 471 (2002).
[32]A. Brandenburg, Astron. Nachr. **332**, 51 (2010).
[33]N. I. Kleeorin and A. A. Ruzmaikin, Magnetohydrodynamics **2**, 17 (1982).
[34]A. Hubbard and A. Brandenburg, Geophys. Astrophys. Fluid Dyn. **104**, 577 (2010).
[35]N. E. L. Haugen, A. Brandenburg, and W. Dobler, Phys. Rev. E **70**, 016308 (2004).
[36]N. Seehafer, Phys. Rev. E **53**, 1283 (1996).
[37]H. Ji, Phys. Rev. Lett. **83**, 3198 (1999).
[38]U. Frisch, *Turbulence. The Legacy of A. N. Kolmogorov* (Cambridge University Press, Cambridge, 1995).